Journal of Physics:
Conference Series

PURPOSE-LED PUBLISHING™

PAPER • **OPEN ACCESS**

Simulation of atmospheric turbulent boundary layers in a wind tunnel using an active turbulence grid

To cite this article: Mahdi Yazdanpanah *et al* 2026 *J. Phys.: Conf. Ser.* **3271** 012009

View the article online for updates and enhancements.

You may also like

- Exchange Current Density of H_2/H_2O Electrode for Reversible Solid Oxide Cells: Theoretical Partial Pressure Dependencies Rate-Determined By Surface Reaction or Transport
Yohei Nagatomo, Ryota Ozaki, Masahiro Yasutake et al.
- Effect of grain boundary on martensite transformation behaviour in Fe–32 at.%Ni bicrystals
Masato Ueda, Hiroyuki Yasuda and Yukichi Umakoshi
- Grain boundary migration in Fe-3mass%Si alloy bicrystals with twist boundary
T Shibayanagi, K Ichimiya and Y Umakoshi

SmarAct | group

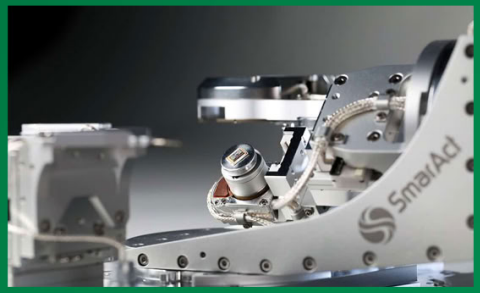
webinar

More details and registration

One sample, many dimensions: prospects for multimodal nanoscale characterization

Explore how precise sample manipulation enables complementary nanoscale techniques to work together on one sample

Live at 2 p.m. GMT/3 p.m. CET,
12 November 2026



This content was downloaded from IP address 144.122.201.61 on 16/11/2026 at 16:51

Journal of Physics: Conference Series **3271** (2026) 012009 doi:10.1088/1742-6596/3271/1/012009

Simulation of atmospheric turbulent boundary layers in a wind tunnel using an active turbulence grid

Mahdi Yazdanpanah[1*], Enes Sertbakan[1], Can Evcimen[1] and Mustafa Percin[1]

[1] Department of Aerospace Engineering, Middle East Technical University, Ankara, Türkiye

[*]E-mail: mahdi.yazdanpanah@metu.edu.tr

Abstract. This study investigates the systematic generation of controlled turbulent boundary layers using an active turbulence grid with a 10×10 array configuration. The experimental setup allows precise adjustment of flow properties to generate customized boundary layer profiles with regulated velocity gradients and turbulence parameters. By modulating the amplitude of the horizontal bars in oscillatory motion and controlling the vertical bars in stationary and single random asynchronous motion patterns, boundary layer profiles representing four distinct surface roughness conditions (α = 0.10, 0.15, 0.175, 0.20) were generated. For each roughness condition, two cases with similar velocity distributions but different turbulence intensity levels (low and high) were examined. The approach effectively decouples mean velocity profiles from turbulence characteristics, enhancing experimental capabilities for atmospheric boundary layer research and wind energy applications.

1. Introduction

Simulating the atmospheric boundary layer (ABL) in a wind tunnel is a fundamental approach for studying the complex flow dynamics of wind as it interacts with built structures and wind turbine farms. It is important to reproduce a boundary layer that realistically mimics the surface roughness of the terrain and the corresponding wind turbulence intensity level. A turbulent boundary layer naturally develops over a surface that requires a long test section to achieve the desired boundary layer thickness. Various techniques are employed to overcome this limitation to accelerate the growth rate of the boundary layer. Among these approaches, passive methods such as spires, roughness elements, and grids [1, 2] and active approaches like jet arrays or floor injection systems [3, 4] have been widely used to enhance boundary layer development in wind tunnels. The introduction of active grids has significantly advanced turbulent flow generation capabilities in wind tunnel testing. Active grids, pioneered by Makita's original research [5], have become widely adopted in wind experiments for generating highly turbulent flows. These devices typically consist of multiple winglets attached to bars, each moving independently in various random motion protocols by stepper or servo motors to produce a range of turbulence characteristics, from shear profiles to gusty flows. Placed at the entrance of the test section, they

Content from this work may be used under the terms of the Creative Commons Attribution 4.0 licence. Any further distribution of this work must maintain attribution to the author(s) and the title of the work, journal citation and DOI.
Published under licence by IOP Publishing Ltd

actively disrupt the incoming flow, forming eddies to generate the specified turbulent characteristics. Comprehensive parametric studies [6, 7] showed that flow gradually achieves homogeneity in transverse planes around 30 mesh size downstream of the active grid. The enhanced flexibility that active grids added to wind tunnel experiments led to remarkable developments in designing and manufacturing. This has resulted in various active grids with notable recent examples including the active grid at ForWind [8] and a substantial active grid at the Norwegian University of Science and Technology (NTNU) [9]. In addition, Bodenschatz et al. [19] developed a unique advanced grid in which each individual winglet is driven solely by its own integrated servo motor, offering finer control of the grid and blockage locally.

Active grids offer the capacity to generate not only nearly homogeneous freestream turbulence but also tailored shear profiles. Shen and Warhaft [11] demonstrated this concept by integrating an active grid with a variable-density mesh and downstream flow straighteners. This arrangement successfully yielded an approximately homogeneous shear flow with $Re_\lambda \sim 1000$; however, the dependence on additional downstream grids and flow straighteners remained a characteristic of their setup. Cal et al. [12] employed an active grid in combination with a series of spires to amplify turbulence intensity and generate shear flows for a model wind farm. However, in this setup, the shear was primarily dictated by the spires and the boundary layer rather than the active grid itself. Cekli and van de Water [13] used a specialized motion protocol to generate boundary layer profiles solely using an active grid. Their approach involved inducing flapping motions in the grid's horizontal bars at predefined angles, dynamically adjusting the blockage across the vertical axis. The vertical bars were rotated randomly to keep constant turbulence intensity. Hearst et al. [14] used an alternative method for shaping shear profiles, utilizing an active grid to generate turbulence using passive and random protocols. This approach influenced the mean geometry of the turbulent boundary layer as it developed over a plate. Despite its advantages, the method was constrained by the shear values and velocity profiles dictated by the wall. Hearst and Ganapathisubramani [15] conducted a more comprehensive analysis of the flow characteristics investigated by Cekli and van der Water [13], employing modified shear-generation protocols. Their goal was to generate similar shear profiles with different turbulence intensities. To achieve this, due to a higher degree of freedom in the horizontal direction, vertical bars were oscillated at predefined angles with random frequencies, controlling shear development. Meanwhile, the horizontal bars modulated background turbulence intensity through passive (fully open position) and three fully random protocols, enabling a range of turbulence conditions. The generated turbulent shear profiles were effective only for the central region of the test section. Furthermore, the preliminary results of our study indicate that this protocol cannot effectively block the flow in boundary layer locations to simulate desired boundary layer profiles.

The present study aims to generate different boundary layer profiles representing distinct surface roughness conditions under varying turbulence intensity levels. To achieve this, it revisits the method introduced by Cekli and van der Water [13], conducting a more detailed examination of the resulting flow characteristics across this systematic range of roughness parameters. In atmospheric turbulent boundary layer simulation, the mean velocity profile over the boundary layer thickness (δ) is commonly expressed as a power law distribution:

$$U(y) = U_\infty \left(\frac{y}{\delta}\right)^\alpha \tag{1}$$

It is known that the power law exponents typically range from α ≈ 0.1 for smooth surfaces to α ≈ 0.3 for highly rough urban terrain. Within this range, the present study focuses on four specific

values: oceanic conditions (α = 0.1), rural environments (α = 0.2), and intermediate surface roughness conditions (α = 0.15, 0.175). The next section describes the experimental facilities, instrumentation, and methods utilized in this study.

2. Methodology

Experiments are conducted in an open-return suction-type boundary layer wind tunnel at the METU Center for Wind Energy Research (RÜZGEM). This wind tunnel features a cross-sectional area of 1 m × 1 m and an 8-meter-long test section. The active turbulence grid used in this study consists of ten horizontal and ten vertical bars, with nine diamond-shaped winglets mounted in the center and two half-winglets mounted on the edges of the rods, yielding a mesh size (M) of 99.4 mm. The winglets are mounted in an alternating configuration along the bars to enhance flow modulation. The active turbulence grid is positioned after the contraction at the entrance of the wind tunnel test section. A two-sensor hotwire rake was designed and deployed for measurements conducted 43 mesh sizes downstream of the active grid. The sensors were spaced 25 mm apart. Figure 1 illustrates the experimental setup, detailing (a) the two-sensor hotwire rake, (b) the schematic of the wind tunnel, and (c) the active turbulence grid in its fully closed position, illustrating the vertical position of each horizontal bar along the Y-axis, referenced in mesh-scale units.

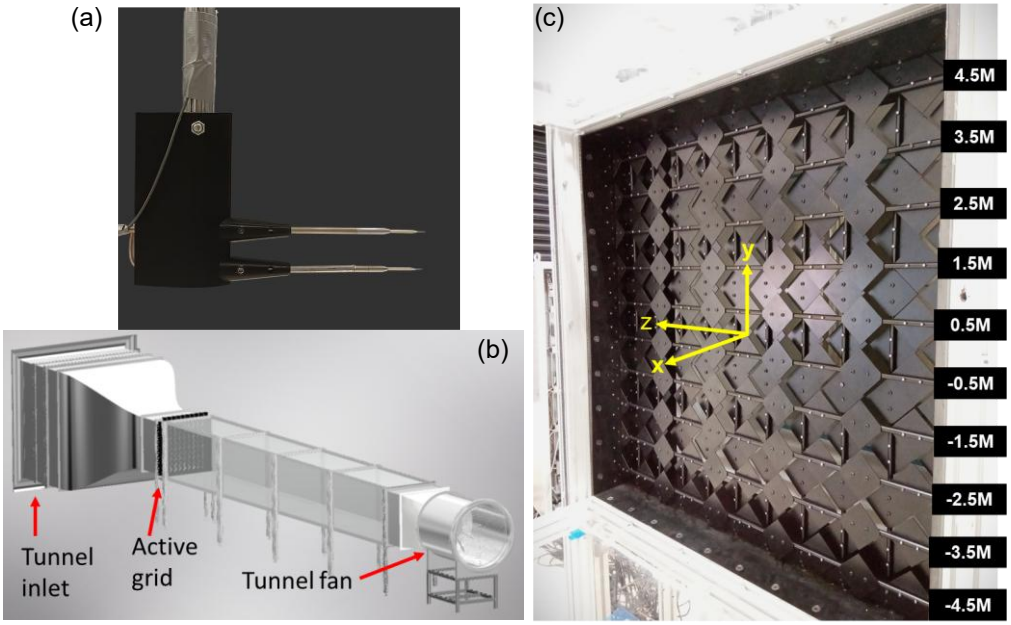


Figure 1. Experimental Setup. (a) Two-sensor hotwire rake used for velocity measurements. (b) Schematic of the open-return wind tunnel and the location of the active grid (c) Active turbulence grid in its fully closed position, with vertical positions of horizontal bars indicated by the mesh-scale units.

Shear was set by adjusting the motion of the horizontal bars. All winglets attached to the horizontal bars were initially set to the predefined angles depending on their horizontal position across the wind tunnel and then oscillated with 5-degree amplitude at a frequency of 2 Hz, except for specific winglets that were kept stationary. The winglet angles were determined by trial and error based on the blockage characterization study. Most winglets were positioned upward toward the incoming flow to thicken the boundary layers.

The vertical bars are responsible for generating turbulent profiles. The double random asynchronous mode categorized by [16] was initially tested. In this mode, both the rotational rate and the duration of rotation (cruise time, after which the direction changes), vary randomly and independently. However, this mode was found to disturb the flow excessively, making the selection of specific angles for the horizontal bars quite challenging. As a result of these observations, the single random asynchronous mode was subsequently selected. In this mode, only cruise time is randomized, following a Gaussian distribution. This mode demonstrated superior control over the flow dynamics. For the turbulent case, a rotational rate Ω = 60 rpm was set, and the lower and upper bounds of cruise time were fixed at 0.1 and 4.1 s, respectively. In the context of the vertical bar motion protocols, A (low turbulence) denotes vertical bars stationary at $\theta = 0°$, and B (high turbulence) denotes vertical bars operating in single random asynchronous mode The four surface roughness conditions are designated as: 1 ($\alpha = 0.1$), 2 ($\alpha = 0.15$), 3 ($\alpha = 0.175$), and 4 ($\alpha = 0.2$). For each condition, two similar boundary layer velocity profiles are generated with different turbulence intensity levels, resulting in eight experimental cases: 1A, 1B, 2A, 2B, 3A, 3B, 4A, and 4B. Table 1 presents the eight boundary layer profile settings with their turbulence modes. The numbers in bold indicate that the winglets are stationary.

Table 1. Boundary layer profile settings and corresponding turbulence modes.

		Horizontal bar position (y)									
Name	α	-4.5M	-3.5M	-2.5M	-1.5M	-0.5M	0.5M	1.5M	2.5M	3.5M	4.5M
1A	0.1	75	38	33	33	22	24	17	10	10	10
1B	0.1	90	80	38	35	25	20	19	10	10	10
2A	0.15	85	48	36	34	24	24	18	10	10	10
2B	0.15	**80**	**80**	-65	24	17	15	15	10	10	0
3A	0.175	90	59	38	36	27	25	19	10	10	10
3B	0.175	**90**	**90**	**-75**	35	27	25	15	10	10	10
4A	0.2	90	-60.5	38.5	29	27	25	15	10	10	10
4B	0.2	**90**	**90**	-85	37	27	24	15	10	10	10

All tests are performed with the fan speed set to achieve an inlet velocity of $U_{inlet} \approx 7$ m/s at the active grid entrance, corresponding to a Reynolds number of $Re_M \approx 41000$. The resulting free-stream edge velocities (U_∞) for the generated profiles range from 7.4 to 7.9 m/s. The rake of two single-sensor hotwire was traversed from y = 25 mm to 875 mm in 17-18 mm increments to cover the range from 25 mm to 900 mm. The sample rate was 20 kHz, and an analog filter was set at 10 kHz. Samples were acquired in one minute, resulting in 1.2 million data points per measurement.

3. Results and discussion

The velocity measurements reveal a complex flow field characterized by three distinct zones within the active grid generated flow field. The first zone represents the simulated turbulent boundary layer region, where the active grid configuration with blocked lower sections and open upper sections successfully creates a velocity profile that mimics natural boundary layer development from the bottom wall. This generated boundary layer is spatially restricted to the wind tunnel test section height, and above the boundary layer edge, the flow field exhibits a

natural response to the active grid momentum manipulation. A momentum recovery zone emerges above the simulated turbulent boundary layer, exhibiting a jet-like velocity distribution resulting from the additional momentum introduced by the open upper grid sections. This jet distribution represents the flow's natural response to compensate for the momentum deficit created by the blocked lower sections. Finally, an interaction zone is observed where the jet flow transitions and settles toward equilibrium, representing the region where the active grid effects diminish and the flow approaches natural test section conditions before encountering the developing top wall boundary layer. This three-zone structure demonstrates how the confined wind tunnel environment constrains the simulated boundary layer generation while the flow field naturally adapts to maintain overall momentum conservation.

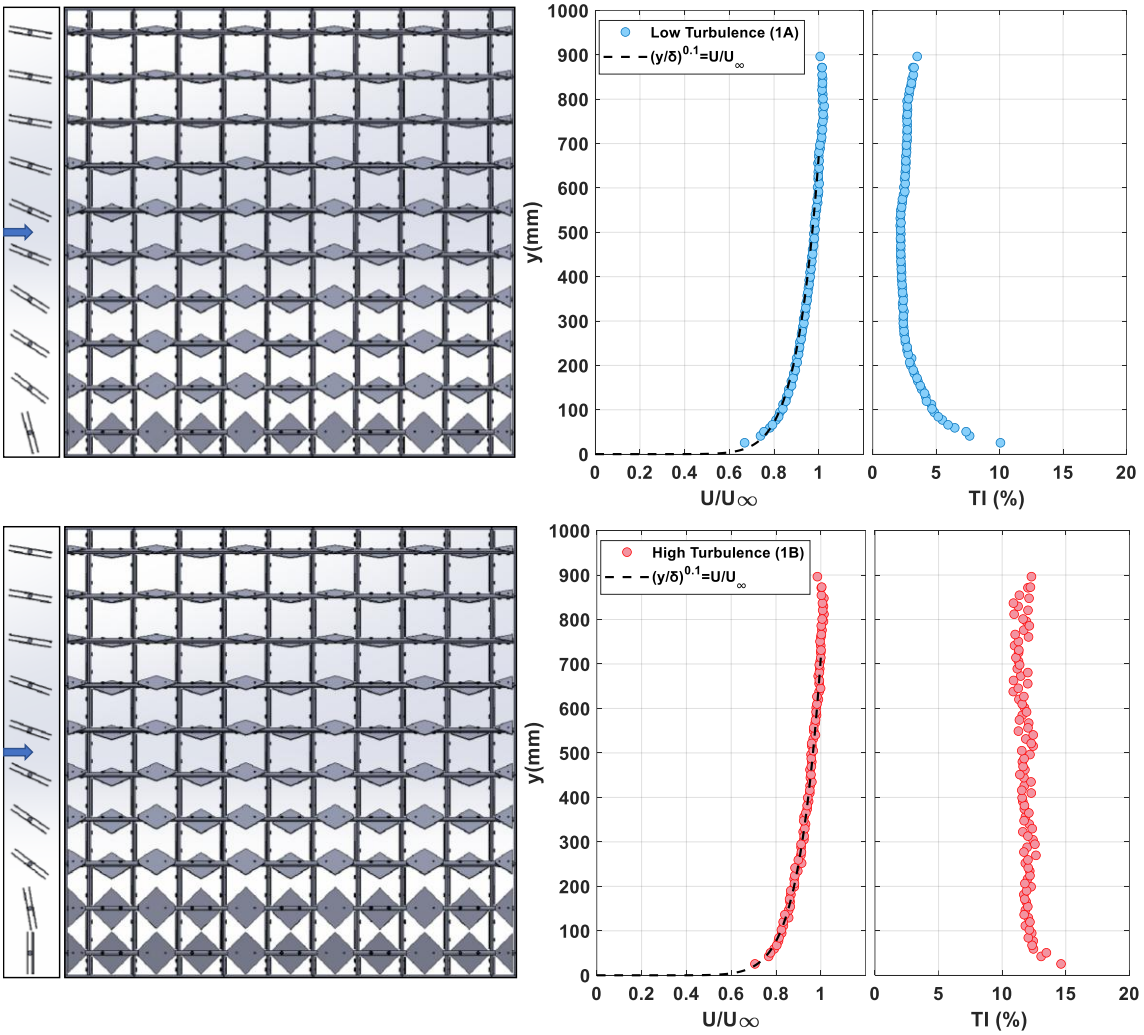


Figure 2. Boundary layer profiles for oceanic conditions (α = 0.1). Top row: low turbulence case (1A, $\delta \approx 67$ cm, U_∞ = 7.4 m/s). Bottom row: high turbulence case (1B, $\delta \approx 71$ cm, U_∞ = 7.6 m/s).

Figures 2-5 present the complete set of generated boundary layer profiles for the four surface roughness conditions investigated. Each figure displays results in two rows with three panels per row: Row 1 (top) shows the low turbulence case (A) and Row 2 (bottom) shows the high turbulence case (B). Each row contains: active grid configuration with side and front views showing flow direction via a blue arrow (left), mean velocity profile with power law fit (center),

and turbulence intensity profile (right). Note that vertical bars are shown in fully open position for both passive and random operational modes for better visualization.

Figure 2 demonstrates successful generation of oceanic boundary layer conditions (α = 0.1) with excellent agreement between measured velocity profiles and the theoretical power law relationship. The turbulence intensity profiles show clearly an increase in turbulence level of approximately 10 percent, from low-turbulence 1A case to high-turbulence 1B case, maintaining similar trend across the vertical direction.

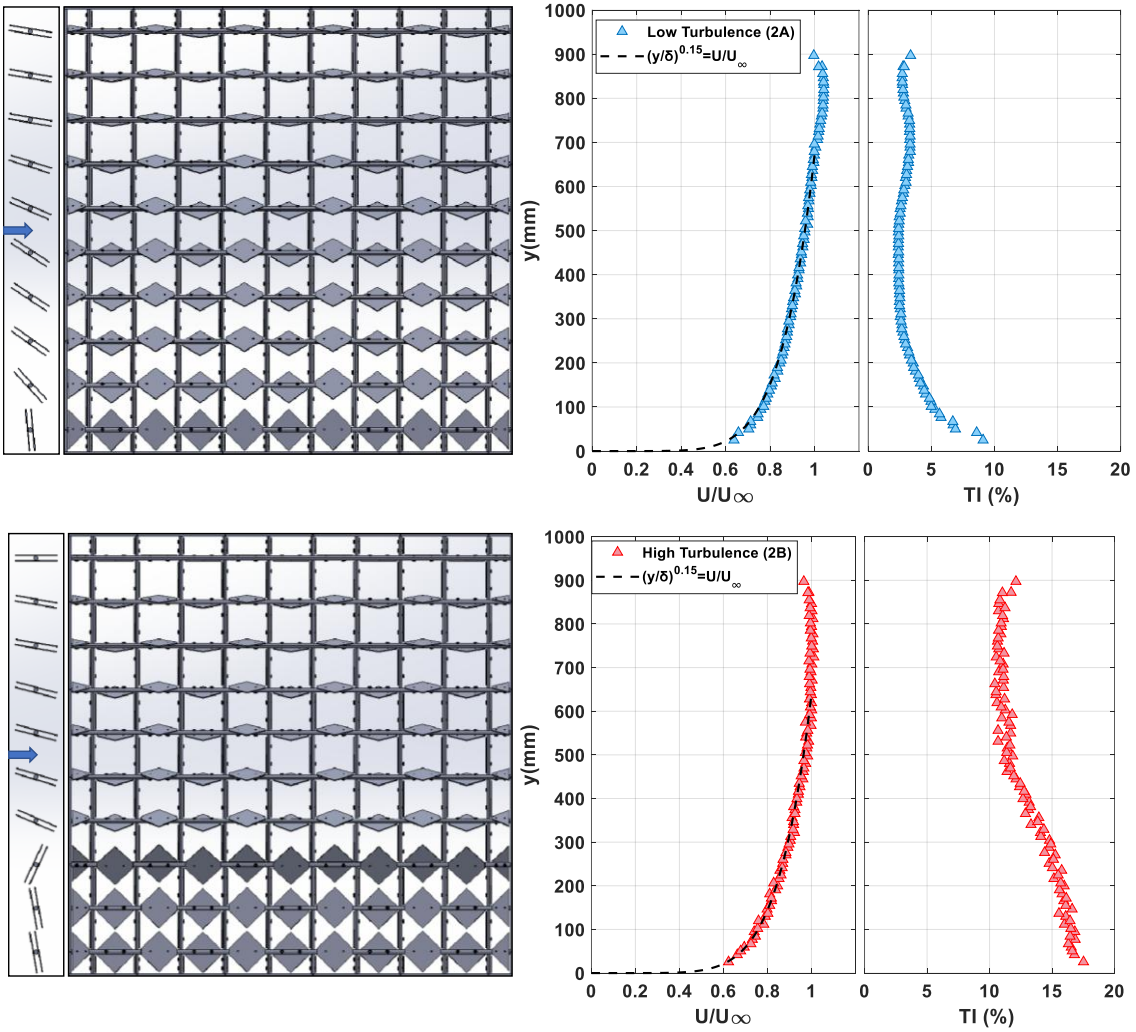


Figure 3. Boundary layer profiles for first intermediate conditions (α = 0.15). Top row: low turbulence case (2A, $\delta \approx 67$ cm, U_∞ = 7.5 m/s). Bottom row: high turbulence case (2B, $\delta \approx 64$ cm, U_∞ = 7.8 m/s).

Figure 3 depicts the first intermediate surface roughness condition (α = 0.15), showing a systematic progression from the oceanic case. The velocity profiles exhibit slightly fuller characteristics compared to α = 0.1, with the power law relationship maintained across both turbulence intensity levels. The turbulence intensity profile of case 2B shows higher values in the lower sections compared to case 1B, primarily due to the third horizontal bar (at y = -2.5M) operating at a negative angle (-65°). It should be noted that these bar angles were initially selected to achieve the desired velocity profile shape (α = 0.15) rather than to intentionally modify the turbulence intensity distribution. However, the negative bar angle creates flow separation and enhanced turbulent mixing as a secondary effect. The -65° orientation specifically generates

significantly higher mixing and turbulence levels compared to the positive angle configurations, demonstrating the strong influence of bar orientation on local flow characteristics This systematic use of negative bar angles to achieve higher α values is consistently applied across cases 2B, 3B, and 4B, with progressively more negative angles (-65°, -75°, -85°). While the more negative angles provide greater blockage effects, the -65° configuration specifically generates the most intense turbulence due to optimal flow separation conditions, resulting in corresponding increases in lower-section turbulence intensity as an unintended but observable consequence.

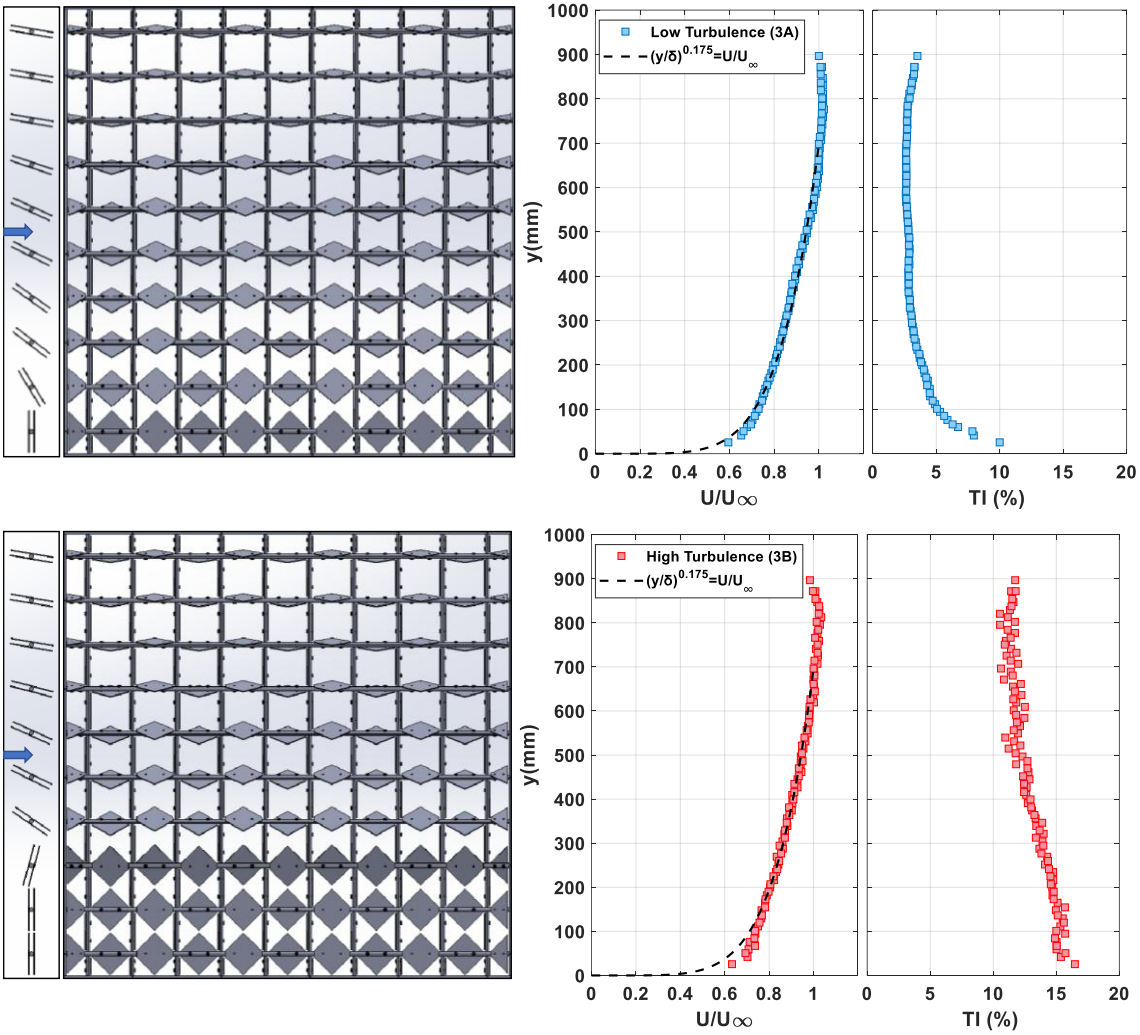


Figure 4. Boundary layer profiles for second intermediate conditions (α = 0.175). Top row: low turbulence case (3A, $\delta \approx 70$ cm, U_∞ = 7.7 m/s). Bottom row: high turbulence case (3B, $\delta \approx 67$ cm, U_∞ = 7.8 m/s).

The velocity profiles in α = 0.175 and 0.2 cases demonstrate a close match to the power-law relations; however, some deviations are observed in the near-wall region (at positions less than one mesh size) due to the inherent challenges in precise flow control at such small scales, a phenomenon consistent with observations in existing literature.

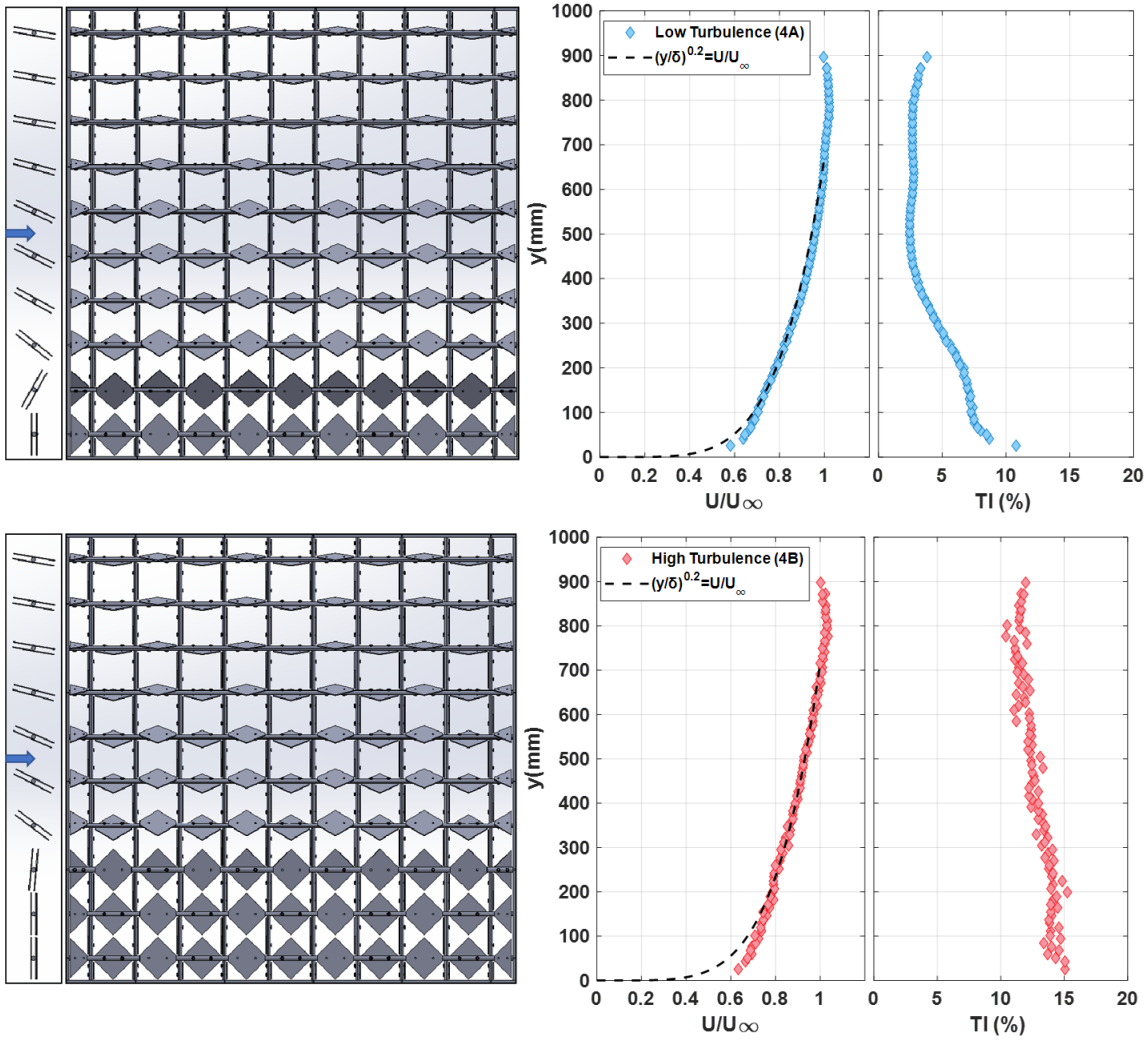


Figure 5. Boundary layer profiles for rural conditions (α = 0.2). Top row: low turbulence case (4A, $\delta \approx 67$ cm, U_∞ = 7.75 m/s). Bottom row: high turbulence case (4B, $\delta \approx 71$ cm, U_∞ = 7.9 m/s).

Classical inner-layer scaling (Law of the Wall) is not considered here, as active-grid-generated boundary layers without downstream roughness elements are not expected to be in equilibrium [13].

4. Conclusions

This work demonstrates that an active turbulence grid with a 10×10 array can systematically generate turbulent boundary layers with tailored velocity and turbulence characteristics. By independently modulating horizontal and vertical bar motions, boundary layer profiles representing surface roughness levels (α = 0.10, 0.15, 0.175, and 0.20) were reproduced while controlling turbulence intensity separately from mean velocity distributions. The experimental results validate the active grid's capability to decouple mean shear profiles from turbulence intensity parameters, enabling independent generation of boundary layer characteristics across multiple roughness conditions. Future work may extend this methodology to higher turbulence intensity levels and varying Reynolds number conditions.

Acknowledgments

The authors would like to thank the METU Center for Wind Energy Research (RÜZGEM) for their support. The active grid used in this study was built with the financial support of the Scientific and Technological Research Council of Türkiye (TÜBITAK) under Project No. 120M497.

References

[1] Counihan J, 1969, An improved method of simulating an atmospheric boundary layer in a wind tunnel, Atmos. Environ., 3, 197–214
[2] Irwin H P A H, 1981, The design of spires for wind simulation, J. Wind Eng. Ind. Aerodyn., 7, 361–366
[3] Teunissen H W, 1975, Simulation of the planetary boundary layer in a multiple-jet wind tunnel, Atmos. Environ., 9, 145–174
[4] Sluman T J, Van Maanen H R E and Ooms G, 1980, Atmospheric boundary layer simulation in a wind tunnel using air injection, Appl. Sci. Res., 36, 289–307
[5] Makita H, 1991, Realization of a large-scale turbulence field in a small wind tunnel, Fluid Dyn. Res., 8, 53–64
[6] Larssen J V and Devenport W J, 2011, On the generation of large-scale homogeneous turbulence, Exp. Fluids, 50, 1207–1223
[7] Hearst R J and Lavoie P, 2015, The effect of active grid initial conditions on high Reynolds number turbulence, Exp. Fluids, 56, 1–20
[8] Kröger L, Frederik J, van Wingerden J W, Peinke J and Hölling M, 2018, Generation of user defined turbulent inflow conditions by an active grid for validation experiments, J. Phys.: Conf. Ser., 1037, 052002
[9] Kildal O, Li L, Hearst R J, Petersen Ø W and Øiseth O, 2023, On the use of an active turbulence grid in wind tunnel testing of bridge decks, J. Wind Eng. Ind. Aerodyn., 233, 105331
[10] Bodenschatz E, Bewley G P, Nobach H, Sinhuber M and Xu H, 2014, Variable density turbulence tunnel facility, Rev. Sci. Instrum., 85, 085501
[11] Shen X and Warhaft Z, 2000, The anisotropy of the small scale structure in high Reynolds number (R $\lambda \sim 1000$) turbulent shear flow, Phys. Fluids, 12, 2976–2989
[12] Cal R B, Lebrón J, Castillo L, Kang H S and Meneveau C, 2010, Experimental study of the horizontally averaged flow structure in a model wind-turbine array boundary layer, J. Renew. Sustain. Energy, 2, 013106
[13] Cekli H E and van de Water W, 2010, Tailoring turbulence with an active grid, Exp. Fluids, 49, 409–416
[14] Hearst R J, Gomit G and Ganapathisubramani B, 2016, Effect of turbulence on the wake of a wall-mounted cube, J. Fluid Mech., 804, 513–530
[15] Hearst R J and Ganapathisubramani B, 2017, Tailoring incoming shear and turbulence profiles for lab-scale wind turbines, Wind Energy, 20, 2021–2035
[16] Poorte R E G and Biesheuvel A, 2002, Experiments on the motion of gas bubbles in turbulence generated by an active grid, J. Fluid Mech., 461, 127–154